Journal of Nuclear Materials 380 (2008) 76–84

Contents lists available at ScienceDirect

Journal of Nuclear Materials

journal homepage: www.elsevier.com/locate/jnucmat

Automated optical microscopy of coated particle fuel

Andrew K. Kercher [a,*], John D. Hunn [a], Jeffery R. Price [b], Pete Pappano [a]

[a] Materials Science and Technology Division, Oak Ridge National Laboratory, Oak Ridge, TN 37831, United States
[b] Engineering Science and Technology Division, Oak Ridge National Laboratory, Oak Ridge, TN 37831, United States

ARTICLE INFO

Article history:
Received 6 May 2008
Accepted 14 July 2008

PACS:
07.60.Pb
28.41.Bm

ABSTRACT

Fundamental technological advances have occurred during the 20 year hiatus in US research on coated particle nuclear fuel. As part of the recent US Department of Energy's Advanced Gas Reactor Fuel Development and Qualification program, Oak Ridge National Laboratory has utilized advancements in computer automation, digital imaging, and image analysis to modernize US optical microscopy techniques for coated particle nuclear fuel. Automated optical microscopy has enabled detailed and objective analysis of individual particles (hundreds of measurements per particle) and of large sample sizes that far exceed the capabilities of conventional manual microscopy methods (analysis of 1500–5000 particles is common). Demonstrative examples of the capabilities of this automated optical microscopy are given for: (a) shadow imaging of kernels, coated fuel particles, and graphite matrix overcoated particles and (b) cross-sectional analysis of coated fuel particles to determine layer thicknesses.

Published by Elsevier B.V.

1. Introduction

As a part of the United States Department of Energy's Advanced Gas Reactor (AGR) Fuel Development and Qualification program, Oak Ridge National Laboratory (ORNL) has recently re-established the US capacity for labscale fabrication and characterization of tri-isotropic (TRISO) coated particle nuclear fuel. A number of important technological advances have occurred during the 20 year hiatus in US coated particle R&D which can be applied to upgrade previous methodology. Perhaps the most significant is the advancements in digital computing over the last several decades. In the effort to improve upon or replace previously used coated particle fuel characterization methods, ORNL has developed advanced procedures for quantitative optical microscopy that utilize computer automation, digital imaging, and advanced image analysis to increase both throughput and accuracy of these measurements.

The coated particle fuel concept involves a spherical kernel of nuclear material surrounded by concentric layers designed to contain the fission products and maintain structural integrity of the particles during fabrication and operation. The coating layers are (in radially increasing order): a low density, porous carbon layer (the buffer); a higher density pyrolytic carbon layer (the inner pyrocarbon or IPyC), a polycrystalline silicon carbide layer (the SiC), and an outer pyrocarbon layer (the OPyC) [1]. The thickness of these coating layers and the diameters of the kernel and coated particle are important parameters that are used to determine that acceptable fuel fabrication has been achieved. The deviations of the kernel and coated particle from an ideal spherical shape are also determined, because abnormal shapes can affect fuel performance and can indicate problems in the fabrication process. Typically, statistical limits are placed on the allowable deviation of these parameters from the target design. Each quality control measurement is made on a representative sample taken from a fabricated material to statistically determine the probable range for the measured parameter in the sampled material.

Quantitative optical microscopy is a standard tool for characterizing and qualifying the size and shape of the particles (both kernels and coated particles) and the thickness of the coating layers. A commonly used method is to utilize a microscopy eyepiece with a reticule to manually measure the dimensions of interest. This technique is so tedious and fatiguing that typical practical limits involve making 1 or 2 measurements per feature of interest and only 100–200 total measurements per inspection. This method is often not adequate to obtain statistically adequate sampling of the material. Manual measurements on photographic images can result in reduced operator fatigue, but photograph processing time is a consideration. Several generic software packages are available for quantitative analysis of digital optical micrographs obtained with today's high resolution digital cameras. Analysis of digital images with generic software packages can enhance measurement accuracy. However, they are still manually executed measurements, and therefore, generic software does not greatly impact operator effort or typical sample sizes. Some off-the-shelf software packages offer automated image analysis and feature recognition, but the capabilities and customizability of these programs are limited.

* Corresponding author. Tel.: +1 865 576 3488; fax: +1 865 574 4186.
E-mail address: kercherak@ornl.gov (A.K. Kercher).

0022-3115/$ - see front matter Published by Elsevier B.V.
doi:10.1016/j.jnucmat.2008.07.011

Recently, several international TRISO R&D programs have developed characterization methods for the size and shape of particles and the thicknesses of coating layers. In Japan as part of the high temperature engineering test reactor (HTTR) program, kernel size and shape have been determined by shadow imaging (100 particle sample for diameter measurement; 300 particle sample for sphericity) and layer thickness has been determined by X-ray radiography [2]. In fuel research for the Chinese high temperature gas-cooled reactor (HTR-10), automated measurements utilizing X-ray radiography and optical ceramography have been coupled with computer data analysis to provide kernel size, kernel sphericity, and layer thicknesses (sample sizes of at least 180 particles) [3]. In the United States, as part of the AGR program, ORNL has transferred the methods described herein to the Babcock and Wilcox Company (Lynchburg, VA) for industrial TRISO fuel development.

The ORNL approach to quantitative optical microscopy of coated particle fuel utilizes computer automated microscope stage movement, digital image acquisition, and image analysis software that was written in-house specifically for analysis of coated particle fuel. Sample sizes of 1500–5000 particles are routinely examined for kernel and coated particle size and shape. For layer thicknesses, routine sample sizes are 180–240 particles. Algorithms identify boundary locations, not subjective judgment. Hundreds of individual diameters or thicknesses are measured per particle. Also, image analysis software has enabled the study of particles using alternative metrics.

2. Experimental methods

Optical microscopy was performed using a Leica DMRx upright microscope with plan fluotar objectives and additional tube magnification optics. Digital micrographs were obtained with a Leica DC500 digital camera system capable of producing up to 12 megapixel images (3900 × 3090 pixels). The microscope was equipped with a motorized stage and a Ludl MAC-5000 automation control system. MediaCybernetics Image Pro Plus software was used to acquire images and was used to perform manual measurements. MediaCybernetics Scope Pro software was used to integrate the stage controller to the image acquisition system for fully automated sample inspection, as described in the following sections. A custom spring loaded mount holder (Fig. 1) was used to quickly and reproducibly align the imaged surface plane parallel to the microscope stage. Fine adjustment screws on the microscope stage insured that a flat mount remained in the focal plane over the entire imaged area to avoid the added complication of automated focusing.

2.1. Size and shape measurements

Particle size and shape can be determined by using the microscope in transmitted bright field mode to produce a shadow image of the optically opaque particle's perimeter. A statistically relevant sample of particles was riffled out of the material using a rotary riffler. Good random sampling procedures are necessary to obtain a sample truly representative of the material. Representative sampling minimizes errors in measurement averages, distributions, and especially distribution tails (crucial for statistical tests based on tolerance limits, discussed later).

Particles were poured inside a washer on a flat clear thermoplastic acrylic mount (Struers Specifast) to make a single layer of loose particles, were covered with a thin glass cover slide, and were loaded into a mount holder (Fig. 1). The loaded mount holder was placed on the microscope stage and was illuminated using transmitted light to create shadow images (silhouettes) of the particles. The choice of nominal magnification depended on the size of the particles (e.g., 80× for ~350 μm kernels (~1.788 pixels/μm), 50× for ~800 μm TRISO particles (~1.118 pixels/μm)). Magnification was decreased for larger particles to obtain sufficient depth of focus and to ensure well defined particle perimeters and sufficient field of view to allow a reasonable number of particles per frame. Magnification was kept as high as possible to provide good resolution (pixels/μm) in the digital image. Transmission light intensity was varied to obtain a transmitted light intensity of 180–220 out of an 8-bit intensity range (0–255). Excessive transmitted light intensity can cause blurring of the edges of particle shadow images and camera pixel saturation should be avoided.

The entire mount of particles was captured with a tiled array of images. Images were analyzed by software written in-house. Each particle was located using grayscale dilation, a distance transform, and watershed segmentation. The software identified the particle centers using a Kasa fit, identified shadow boundary positions (searches at 1° intervals), and used the fast Fourier transform (FFT) to obtain a low-frequency parametric representation of the boundary shape (Fig. 2). Specific details of the software analysis can be found in other publications [4,5]. By identifying the particle center and obtaining a parametric representation of the boundary, various size and shape metrics could be calculated, such as average particle diameter, average particle radius, diameter aspect ratio (the maximum diameter divided by the minimum diameter), radius aspect ratio (the maximum radius divided by the minimum radius), and curvature metrics. Particles with the highest diameter aspect ratios were automatically saved to a separate folder for manual review after processing. This manual review served as a check on the image analysis algorithm as well as an inspection of the most abnormal particles.

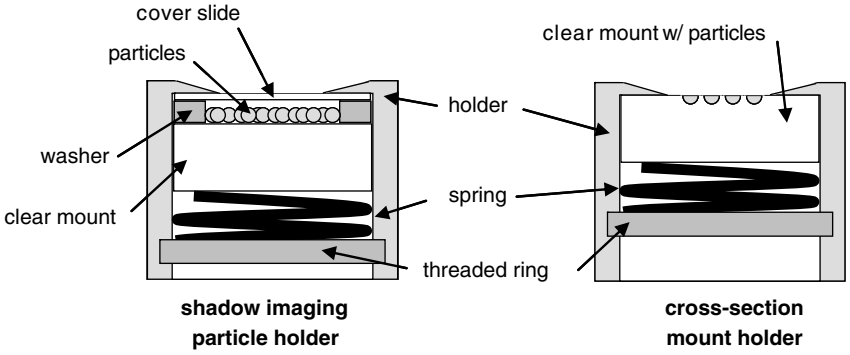

Fig. 1. Schematics of mount holders used for shadow imaged particles and cross-sectioned particles.

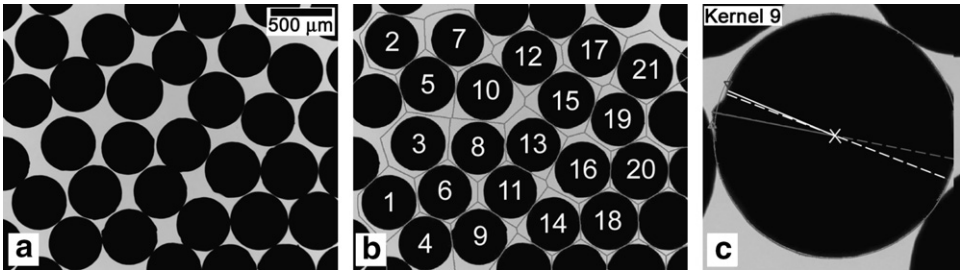

Fig. 2. Stages of the shadow image program analysis: (a) original digital image of kernels (LEU03), (b) individual particles identified by program for analysis, and (c) example result from analysis. Shown in (c) are the particle boundary (small gray points), the particle center (white ×), circle of average radius (gray circle), minimum radius and diameter (white solid and dashed lines), maximum radius and diameter (gray solid and dashed lines), and points of high and low curvature (triangles).

Typically, a single operator working alone could complete full characterization of ~1600–1800 TRISO particles with a one day turnaround: 5 h doing sample preparation and image acquisition (6 holders, 56 tiled images per holder), 12 h of computer time to analyze particles in tiled images (usually performed overnight without human interaction using a single Intel Xeon CPU at 2.80 GHz with 3 GB of RAM), followed by 3 h to review high aspect ratio particles and complete a standardized statistical report on sizes and aspect ratios.

2.2. Coating thickness measurements

2.2.1. Mounting and polishing particles for cross-sectional analysis

The layer thicknesses in TRISO-coated particles were determined by microscopy measurements of polished cross-sections of mounted particles. A sample of particles for cross-sectioning was taken randomly from a small riffled quantity of material. To enable subsequent automated image acquisition, particles were arranged in a roughly square array using a polyethylene or polypropylene mesh (1 mm^2 openings) and mounted in a clear thermoplastic acrylic (Struers Specifast). An 11 × 11 square piece of plastic mesh was used. The plastic mesh was pressed in a hot press (Struers ProntoPress-10) at 100 °C in order to obtain a mesh that was less than 330 μm thick (less than half the average particle diameter). Typically, 80 particles were placed on the bottom ram of the press in the central 9 × 9 squares of the mesh with one corner left empty as an index. All particles would be touching the flat bottom ram. Twenty cubic centimeters of thermoplastic acrylic powder were poured gently into the press on top of the particles and mesh. The mount was pressed by the following schedule: 15 min with no pressure at 180 °C to completely liquefy the thermoplastic followed by 15 min at 30 kN with slow cooling to 100 °C to surround the particles and allow the resin to solidify. This pressing schedule was developed to minimize axial stresses on the particles during pressing (axial stresses transferred through the powder can result in fractured coatings). The mount was further cooled to room temperature before removing from the press. Mount thicknesses were measured at four particle locations before, during, and after polishing by a calibrated Starrett height gauge using a 3 mm ruby ball gauge tip (0.001 mm resolution; measurement uncertainty 0.002 mm).

The mount was ground using a Struers ALLEGRO disk with 9 μm diamond suspension at 140 rpm and 30 N of force until the polish plane was within 50–70 μm of the average particle midplane (at which point the plastic mesh had been completely removed). The mount was then sonicated in isopropanol to remove grinding debris. The mount was then polished using a Struers DAC disk with 3 μm diamond suspension at 140 rpm and 20 N of force.

2.2.2. Imaging and analysis of particle cross-sections

A polished mount was loaded into a mount holder (Fig. 1), was placed on the microscope stage, and was aligned with the empty corner of the mesh grid at the upper left corner of the stage. The mount was illuminated with both reflected and transmitted light. Illumination intensity and exposure conditions were adjusted so that the maximum reflected light intensity and maximum transmitted light intensity were both 180–220 out of an 8-bit intensity range (0–255). Consistent illumination conditions aided the subsequent image analysis. The focus on the polished surface was optimized for the entire array of particles.

Image Pro macros were used to define the coordinates of the particles in the three corners of the particle array, estimate all particle locations using a parallelogram grid, and perform automated image acquisition of particles based on the parallelogram grid. Occasionally particles were not fully contained in images using these estimated particle locations; any such particles were manually reimaged without readjusting light or focal conditions. A rough measurement of layer thicknesses and kernel radii of a few particles was performed using Image Pro measurement tools.

An in-house written program was used to radially unwrap particle cross-section images in order to identify layer interfaces at 1° intervals and determine kernel radius and layer thicknesses. Because of the microstructural variability of certain kernel types, a preprogram was run to identify the approximate kernel center and one kernel edge point for each image. These approximate coordinates were used to obtain the kernel perimeter points by the Kasa method. Additional program inputs included image resolution (~2.827 pixels/μm, for the example in this paper), approximate average layer thicknesses and kernel radius, polish-down distance measured at the coordinates of the four mesh corners, and kernel type. Approximate average layer thicknesses and kernel radius were used in the program to avoid the identification of anomalies as layer boundaries (e.g., SiC delaminations inside layers or porosity bands in the buffer or pyrocarbon layers). The entered approximations do not have to be particularly accurate (within ~10 μm for buffer thickness and ~4 μm for other layers) and do not bias the results. Polish-down distance for each individual particle was calculated based on an analytical fit of the polish plane using measurements at four particle locations. Layer thicknesses were calculated by the following equation (variables defined in Fig. 3; details given in Section 4.3) which uses polish-down distance to correct the radial positions of layer boundaries for bias caused by off-midplane polishing:

$$t = \sqrt{r_{m2}^2 + \left\{\frac{1}{4p^2}(R_m^2 - p^2)^2\right\}} - \sqrt{r_{m1}^2 + \left\{\frac{1}{4p^2}(R_m^2 - p^2)^2\right\}}. \quad (1)$$

Layers of particles appear thicker when polished off-midplane, because they are viewed at an angle to the radius. Imaging off-midplane is unavoidable, because the coated particles have a significant particle size distribution (in the AGR program, TRISO particle batches of ~400 μm radius had a standard deviation of ~7 μm). Kernel type was specified (uranium oxide or uranium carbide), because different kernels caused sufficiently different

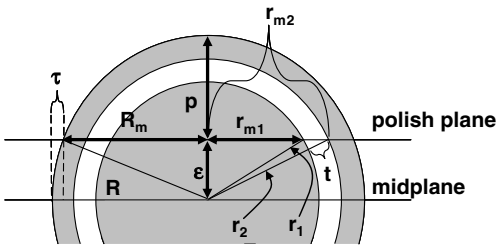

Fig. 3. Layer thicknesses as imaged off-midplane differ from actual thicknesses, but can be corrected geometrically.

appearances at the kernel/buffer interface to require minor changes to the boundary identification algorithm. Further details of the layer thickness program can be found in other publications [4,5].

The layer thickness program saved to a folder reduced resolution images of every particle with the identified boundaries indicated. These reduced resolution images were manually inspected for significant errors in boundary location. The most common errors in boundary location were caused by: skipped boundaries, fragmented buffer/kernel boundaries, or indistinct outer boundaries. A particle with a layer thickness dramatically thinner than the layer thickness estimate could result in a failure to identify that boundary. If kernels were significantly friable at the buffer interface, resulting in crumbling and pull out in this region during sample preparation, the buffer/kernel boundary could be sufficiently fragmented as to prevent accurate boundary determination. The outer particle boundary was sometimes indistinct due to polishing damage around a localized shape anomaly. All these errors were easily identified by perusing the reduced resolution images. Images with skipped boundaries were not discarded, but were rerun with revised layer estimates, because selectively discarding particles which may have abnormally thicker or thinner layers would affect the tail of the layer thickness distribution. Any faulty data due to boundary location errors were deleted.

Typically, a single operator working alone could complete full characterization of one 80 particle mount according the following time estimates: 1 h to align and image each mount, ½ h of manned computer time per mount for identifying kernel coordinates using the preprogram, 4 h of unmanned computer time per mount for analysis by layer thickness program (using a single Intel Xeon CPU at 2.80 GHz with 3 GB of RAM), followed by 2 h to peruse low resolution images, take appropriate actions for boundary errors (rerun images and/or deleting bad data), and complete a standardized statistical report.

3. Results

This section reviews typical results from small comparative studies for shadow imaging and cross-sectional analysis. These comparative studies illustrate how the automated microscopy methods provide detailed property distributions that enable valuable property differentiation between different materials.

3.1. Shadow imaging of kernels

During process development in the AGR program, several different kernel types have been used, starting with surrogate zirconium oxide spheres, then depleted uranium oxide kernels (DUO), natural uranium carbide/uranium oxide kernels (NUCO) and finally, low enriched uranium carbide/uranium oxide kernels (LEUCO) for irradiation testing in the Idaho National Laboratory Advanced Test Reactor. Shadow imaging of these different kernels provided size and shape data needed for kernel production feedback, input for coating processing, and further coated particle characterization.

Automated shadow imaging has allowed detailed histograms of kernel sizes and shapes to be created for the various kernel materials. Histograms for mean particle diameter and diameter aspect ratio (maximum particle diameter divided by the minimum particle diameter) are shown for 350 μm NUCO kernels in Fig. 4. Control of kernel size and shape is essential for producing a consistent TRISO-coated product. Coating rate has been observed to be dependent on the surface area of the substrate. Small kernels tend to receive thicker coatings when mixed with larger kernels. Minor shape irregularities can be 'smoothed out' by the buffer coating, but severe shape irregularities often propagate throughout the coating process to produce layers with high stress regions (Fig. 5). Non-spherical kernel shapes can often be related to defective or non-ideal kernel microstructures.

For TRISO particles under irradiation, failure fractions for high quality fuel have been around 6×10^{-5} or better [6,7]. Thus, the tail of a shape metric distribution (for kernels or coated particles) could have a strong impact on the failure fraction of a TRISO material under irradiation if the non-spherical shape leads to increased probability of particle failure. Superior understanding of distribution tails requires an automated measurement technique. Cumulative distributions of four kernel materials from the AGR program are shown in Fig. 6. The uranium oxide kernels, which are easiest to manufacture, were clearly the most spherical. The uranium carbide/uranium oxide kernels showed improvement during the chronological progression from NUCO to LEUCO-3.

3.2. Shadow imaging of graphite matrix overcoated TRISO particles

High temperature gas-cooled reactor fuel compacts (cylinders and spherical pebbles) consist of TRISO particles embedded in a graphite matrix. These are formed by overcoating TRISO particles with a graphite matrix resin and then pressing the final fuel shape [8]. Shadow imaging was used to optimize the overcoating process used by the AGR program. For example, Fig. 7 shows how the overcoated particle diameter and diameter aspect ratio varied with overcoater rotation speed. If small sample sizes were tested, the 700 rpm overcoated material would be difficult to differentiate from overcoated materials made at higher rotation speeds. By using automated methods to analyze samples with hundreds of particles, overcoater rotation speed up to 1400 rpm could be observed to further narrow overcoated particle size distribution and to further decrease the fraction of material with high diameter aspect ratio.

Shadow imaging generally assumes a random orientation of each silhouetted particle. Kernels and TRISO particles had sufficiently low diameter aspect ratios, such that particles mounted for shadow imaging did not have a noticeable preferred orientation. The lack of preferred orientation was confirmed by comparing normal shadow imaging with shadow imaging of particles poured randomly onto a transparent sticky surface, where reorientation of the particles would not occur. When particles are significantly non-spherical, as is the case for some overcoated particles, preferred orientation during shadow imaging analysis can be expected and must be accounted for when analyzing these materials.

3.3. Layer thicknesses of TRISO particles

Even with meticulous polishing techniques, accurate layer thickness measurements required correction of measured layer thicknesses for off-midplane polishing, which is affected by the particle size distribution, the average polish distance, and the uniformity of polish across a mount. Detailed discussion of the mathematical correction for off-midplane polishing is discussed in Section 4.3. This section provides a typical example of layer thickness data produced by automated microscopy using off-midplane

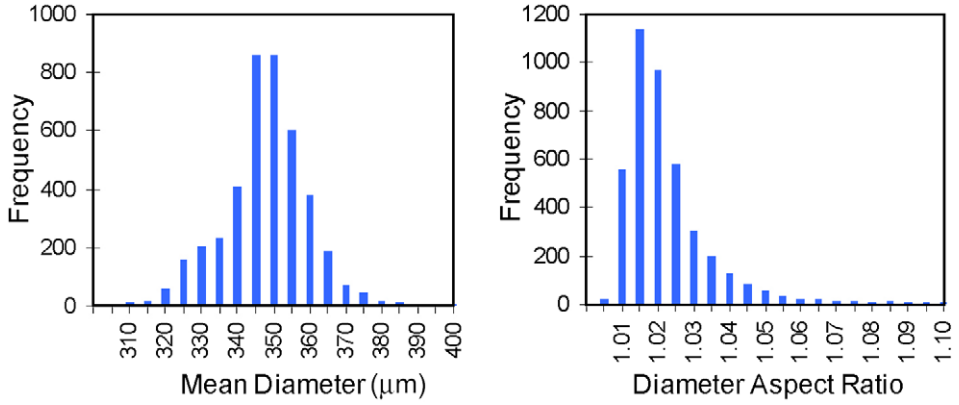

Fig. 4. Results of shadowgraph analysis of 4196 nominally 350 μm diameter NUCO kernels. Average diameter was 345 μm with a standard deviation of 15.2 μm. Thirty-six kernels were less than 300 μm, and 22 kernels were greater than 400 μm. Thirty kernels exhibited a diameter aspect ratio greater than 1.1. Horizontal axis labels show upper limit of bin.

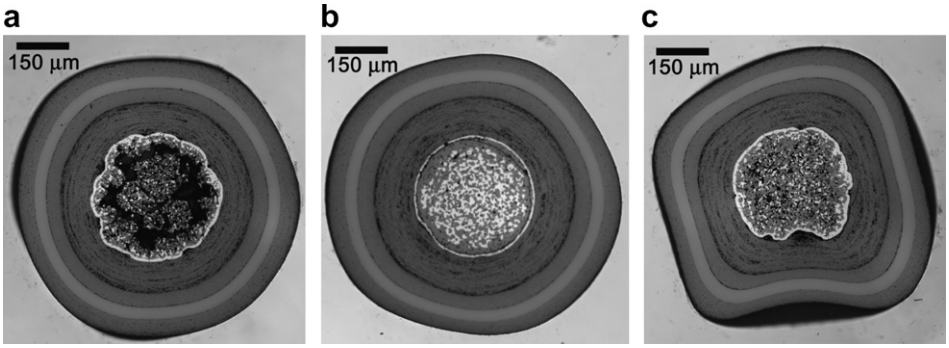

Fig. 5. The buffer coating can 'smooth out' shape irregularities in the kernel (a and b), but severe shape irregularities often propagate through all of the coatings (c). Note that the full severity of kernel irregularities may not be seen in cross-sections. (Cross-section images were from a composite material of TRISO-coated 350 μm NUCO kernels).

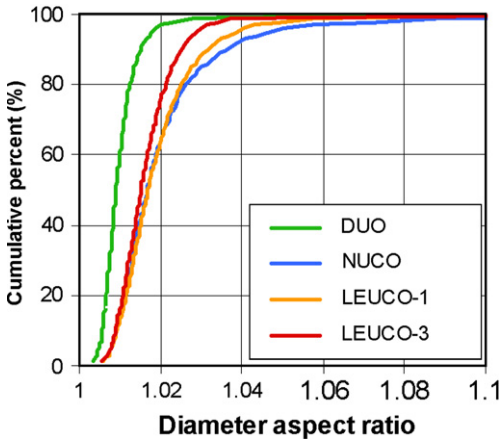

Fig. 6. Cumulative percentages of diameter aspect ratio for four different types of kernels (each nominally 350 μm): depleted uranium oxide (DUO), natural uranium carbide/oxide (NUCO), and two versions of low enriched uranium carbide/oxide (LEUCO-1 and LEUCO-3).

correction based on Eq. (1). Special focus is placed on mount to mount uniformity of the buffer thickness, since it is the most sensitive layer to measurement variability. Thickness data on four TRISO batches with identical processing conditions (on LEUCO-3 kernels) and a composite made from nearly equal amounts of these four materials will be used to provide an example of the automated optical microscopy technique.

Three mounts of 80 particles each were analyzed for each of the five materials (four individual materials and their composite material). Table 1 provides buffer thickness data for these materials. Due to boundary recognition errors (mainly associated with severely chipped kernel/buffer boundaries), no mount had all 80 particles measured for buffer thickness. No correlation has been found between layer thicknesses and features that result in layer data deletion, so final layer thickness means and distributions were not affected. For every mount, the standard deviation of corrected measurements was lower than the standard deviation of uncorrected measurements. For any one of the five materials, statistical comparison of buffer thickness measurements revealed only slight measurement biases from mount to mount. Measured statistically significant variability was found more frequently between mounts of different batches, but this variability may have partially been due to true slight variability of buffer thickness between batches. Histogram results for all layers of the composite material are provided as an example of final results from the automated optical microscopy method (Fig. 8). Layer thickness histograms usually have a Gaussian-like shape. The thickness distributions from individual mounts overlapped extensively for the composite material.

4. Discussion

Acceptance criteria associated with TRISO fuel materials are based on demonstration that particle lot properties fall within specified statistical confidence ranges for the various properties. Computer-automated quantitative optical microscopy enables the practical use of larger sample sizes for this analysis, compared to

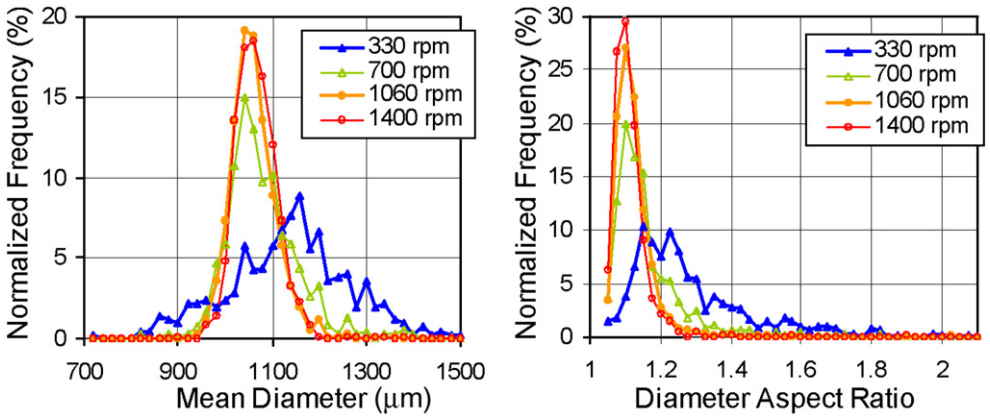

Fig. 7. Histograms (top-binned) of mean diameter (μm) and diameter aspect ratio for overcoated TRISO particles created at different overcoater rotation speeds.

Table 1
Buffer thickness data was calculated for five different TRISO materials

Material		Buffer thickness (avg. (st. dev.) in μm)			
		Mount 1	Mount 2	Mount 3	Total
1	Corrected uncorrected # measured	113.9 (8.3) 115.7 (9.2) 64	110.0 (8.1) 114.0 (8.9) 63	109.6 (7.7) 111.7 (8.4) 60	111.2 (8.2) 113.8 (8.9) 187
2	Corrected uncorrected # measured	109.1 (9.0) 110.9 (9.7) 73	108.9 (7.6) 109.7 (7.9) 55	109.2 (9.1) 111.5 (10.1) 76	109.1 (8.6) 110.8 (9.4) 204
3	Corrected uncorrected # measured	111.7 (8.6) 112.4 (8.9) 79	112.7 (7.9) 114.0 (8.2) 78	110.6 (8.2) 111.4 (8.6) 78	111.7 (8.2) 112.6 (8.6) 235
4	Corrected uncorrected # measured	114.1 (7.9) 115.1 (8.3) 76	112.1 (8.7) 113.6 (9.3) 79	114.1 (7.6) 114.4 (7.8) 77	113.4 (8.1) 114.3 (8.5) 232
Composite:	Corrected uncorrected # measured	109.7 (8.8) 109.8 (8.8) 61	109.5 (6.4) 110.1 (6.6) 71	110.1 (8.1) 110.2 (8.1) 60	109.7 (7.7) 110.0 (7.8) 192

Thickness measurements were corrected for being measured off from particle midplane. Three mounts of each material were analyzed.

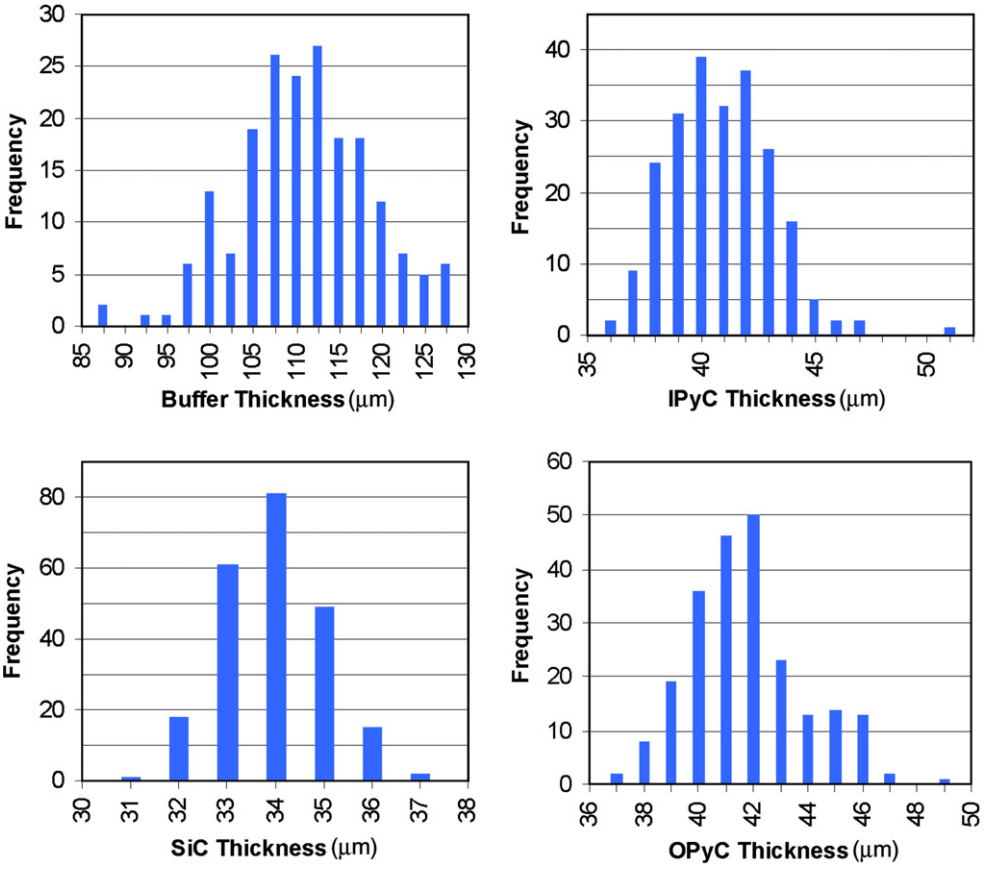

Fig. 8. Histograms (top-binned, in μm) of layer thicknesses for a composite material (with LEUCO-3 kernels).

manual methods. Sections 4.1 and 4.2 present examples of how computer-automated quantitative optical microscopy can greatly narrow confidence ranges for measured properties. Section 4.3 discusses uncertainty analysis of layer thicknesses measurements with a focus on off-midplane correction.

4.1. Statistical analysis of shadow imaging data for TRISO particles

For size and shape measurements on TRISO particles using shadow imaging, typical critical performance parameters are: mean diameter, diameter aspect ratio, and sometimes diameter dispersion. The benefits of the computer-automated optical microscopy method will be described for statistical tests of mean diameter and diameter aspect ratio on AGR-1 baseline TRISO particles (see Fig. 9).

A confidence interval for the mean particle size of a lot can be calculated using student-T statistics:

$$\bar{x} - \frac{t_2 \sigma_x}{\sqrt{n}} \leqslant \mu_e \leqslant \bar{x} + \frac{t_2 \sigma_x}{\sqrt{n}}, \tag{2}$$

where μ_e is the expected mean of the material lot, $\bar{x}$ and σ_x are the measured mean and standard deviation of the analyzed sample, t_2 is the two-tailed student-T statistic for the desired confidence level, and n is the number of particles in the sample. For the 1626 TRISO particles measured for AGR-1 baseline TRISO, the 95% confidence interval for mean diameter was 799.1–800.2 μm. If the same mean and standard deviation were measured for a sample size of 100 (a relatively large sample size for manual measurement), the 95% confidence interval would be 797.4–802.0 μm. In a production environment, a narrower confidence interval for a pertinent mean property often equates to a superior understanding of product and process variability and a higher percentage of product runs passing a specified acceptance criteria.

For diameter aspect ratio of kernels or coated particles, attribute sampling is commonly used to calculate whether (to a specified confidence level) less than a specified fraction of the material (the tolerance limit, L_t) has an aspect ratio greater than a specified value (the control limit). Attribute testing uses the following equation based on the binomial distribution [9] (if the sample size approaches the entire amount of the material, then a hypergeometric distribution should be used):

$$L_c = 1 - \sum_{i=0}^{n_d} \frac{n!}{i!(n-i)!} L_t^i (1 - L_t)^{n-i}, \tag{3}$$

where L_c is the calculated confidence level, n is the number of particles analyzed (sample size), and n_d is the number determined to be defective (based on the control limit).

The tolerance limit chosen for acceptance criteria can be limited by the practical sample size for testing. At best (with zero particles measured to exceed a control limit), a sample size of 50 can only show to 95% confidence that the entire lot has less than 5.82% beyond the control limit. A sample size of 299 particles, which would be extremely laborious by manual methods, is necessary in order to have 95% confidence that less than 1% of a lot is beyond a control limit (with zero particles measured to exceed the control limit). This limitation is solely a result of the statistics in Eq. (3) and is not related to the quality of the product. The result is a need to analyze larger numbers of particles in order to be able to demonstrate product acceptance to low tolerance limits. If failures are detected then the required number of particles that need to be analyzed may even be greater. For the baseline TRISO sample of 1626 particles analyzed by automated shadow imaging, a tolerance limit of 0.00185 (0.185%) could be shown to 95% confidence if zero particles were measured to exceed the control limit. As previously mentioned, failure fractions for irradiated high quality fuel have been around 6×10^{-5} or better. Computer-automated optical microscopy may enable tolerance limits for diameter aspect ratio (or some other shape metric) to not merely be used as a statistical tool for quality assurance; tolerance limits may be able to be set sufficiently low, so that models can predict an expected failure fraction during irradiation based on a calculated tolerance limit for pre-irradiated fuel shape.

4.2. Statistical analysis of layer thickness data

The average layer thicknesses of TRISO particle production lots must statistically be proven to lie within specified acceptable ranges to be suitable for commercial use; statistical tests (such as discussed in Section 4.1) can be used to determine whether the measured average layer thicknesses of a sample allow the lot to pass the acceptance criteria to a specified confidence level (often 95%). A large sample size increases the confidence level that the material lot passes specification, if the sample has a measured average layer thickness within the specified range. TRISO material lots must sometimes also pass dispersion specifications on the acceptable percentage of particles that have layer thicknesses beyond specified limits (to a given confidence level). An example of a dispersion test on layer thickness is given below.

Normal (Gaussian) parametric testing of a distribution involves: (a) calculating the tolerance limit for which it can be stated (with a specific statistical confidence) that only a certain percentage of the sample exceeds it and (b) comparing the calculated tolerance limit with acceptable dispersion specifications. The equations for one-sided tolerance limits are [10]:

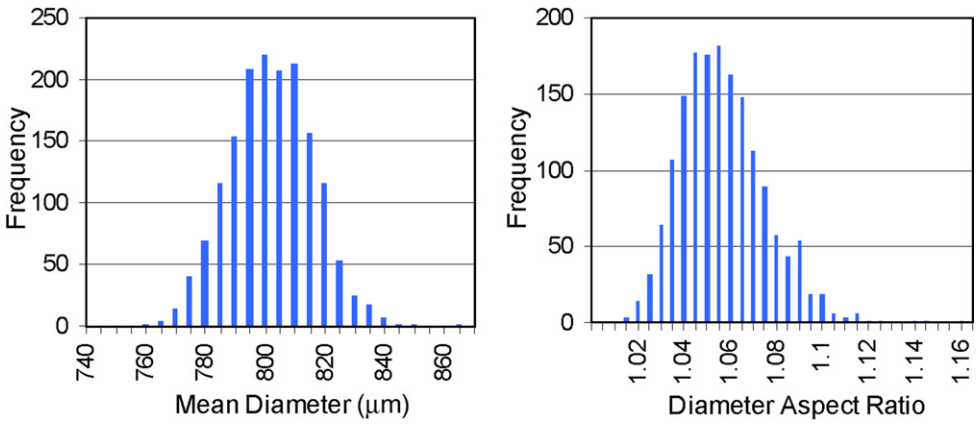

Fig. 9. Histograms (top-binned) of mean diameter (in μm) and diameter aspect ratio for AGR-1 baseline TRISO particles (1626 particles measured in sample).

$$R_L = \bar{x} - K_1\sigma_x, \tag{4}$$

$$R_U = \bar{x} + K_1\sigma_x, \tag{5}$$

where $\bar{x}$ is the mean, σ_x is the standard deviation, K_1 is the one-sided tolerance factor, R_L is the lower tolerance limit, and R_U is the upper tolerance limit. For a composite batch of TRISO material (same as in Section 3.3, Fig. 8, and Table 1), the calculated upper and lower tolerance limits for each layer of the composite batch to have less than 5% of the particles exceeding the limit at 95% confidence were (K_1 factor for 5% at 95% conf. = ~1.84):

- Buffer: R_L = 95.5 μm; R_U = 123.9 μm
- IPyC: R_L = 36.2 μm; R_U = 44.6 μm
- SiC: R_L = 31.5 μm; R_U = 35.5 μm
- OPyC: R_L = 37.5 μm; R_U = 45.1 μm

The sample size was sufficiently large that nonparametric testing (using Eq. (3)) could be used, but the corresponding nonparametric tests for each layer provided results sufficiently close to be within the measurement uncertainty of the analysis.

4.3. Uncertainty analysis of layer thickness measurements

Optical microscopy of polished mounts of TRISO-coated particles inherently involves five fundamental issues. (1) Due to the size distribution of as-manufactured TRISO materials, it is not possible for all particles in a mount to be polished to midplane. For example, the size distribution of TRISO materials measured for the AGR program after rolling and tabling typically had a standard deviation of ~7 μm in radius, so the particle diameters in an 80 particle mount would vary from average radius by approximately ±15 μm. (2) Precision polishing a mount of TRISO particles is a daunting challenge. Tight control of mundane features (e.g., mounting ram flatness, sample alignment during polishing, cooling time in the mounting press) significantly improved polishing precision, but mount polishing under strict standards still produced significant variability across a mount and between mounts. (3) The direction of true thickness (normal to the layer surface) at a particle aspherical feature is unknowable by cross-sectional microscopy, so locally the apparent layer thickness at an aspherical feature can be greater or less than the apparent layer thickness for nearly spherical regions. (4) Radial thickness measurements on a single particle cross-section often vary significantly; for ORNL TRISO materials with 350 μm kernels, average standard deviations of layer thickness measurements of individual particles were typically ~4–5 μm for buffer, ~2–3 μm for IPyC, ~1–2 μm for SiC, and ~2–3 μm for OPyC. Therefore, a small number of manual thickness measurements per particle is highly prone to measurement biases.

Additional measures must be taken to minimize the effect of the fifth issue: thickness measurements on approximately spherical particles polished off-midplane. A cross-section of a perfectly spherical TRISO-coated particle provides a distorted view of the radial positions of the layer boundaries (relative to the true particle center) unless the polish plane is at the midplane of the particle (Fig. 3). Radially innermost layer boundaries are most affected by this distortion. Layer thickness (t) for a spherical particle polished off-midplane can be calculated by the following equation which uses the off-midplane distance (ε) to adjust the as-measured radial positions of the layer boundaries (symbols are defined in Fig. 3):

$$t = r_2 - r_1 = \sqrt{r_{m2}^2 + \varepsilon^2} - \sqrt{r_{m1}^2 + \varepsilon^2}. \tag{6}$$

Fig. 10 shows the percentage error of kernel diameter and layer thicknesses as a function of off-midplane distance (ε).

The off-midplane distance cannot be directly measured with sufficient accuracy using optical microscopy, so one must choose a mathematical expression to calculate (or substitute for) off-midplane distance. Early published work on the AGR program [5] calculated ε from the parameter τ, which is the distance from the edge of the OPyC in the polished plane to the outermost visible edge of the particle, which appears as a shadow in the transparent epoxy mount when illuminated from the back (see Fig. 5 for example). In order to minimize the necessary correction, particles should be polished as close to the average midplane as possible. However, no shadow is visible for a particle polished beyond its midplane. For this reason, in practice, the shadow thickness

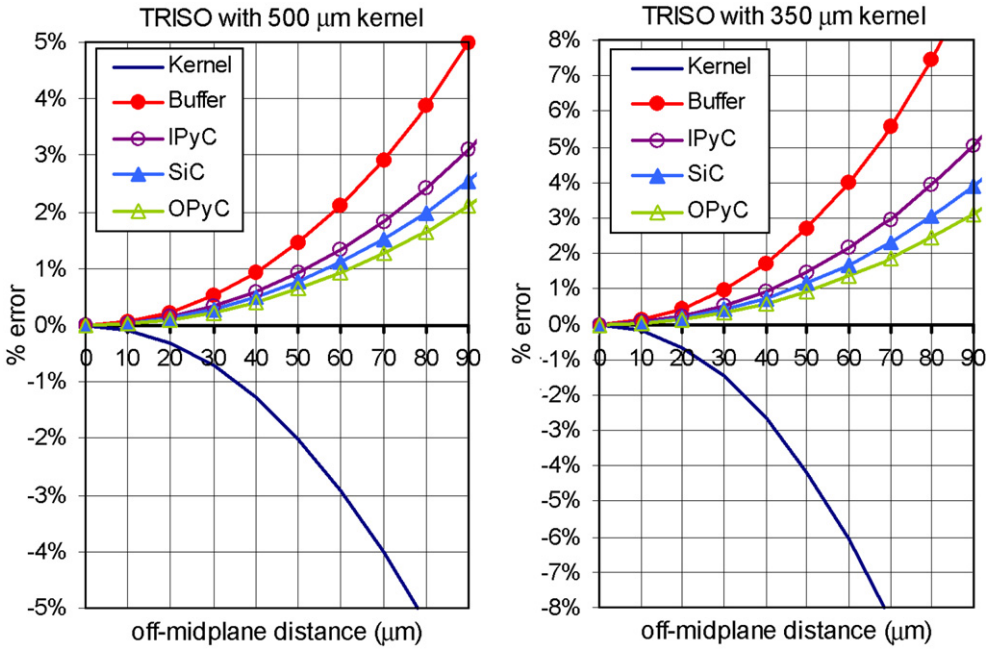

Fig. 10. The percent error of as-measured layer thicknesses and kernel diameter for two spherical TRISO materials as a function of off-midplane distance (ε).

measurements required a large average off-midplane distance so that very few particles in the mount were overpolished and 'shadowless'. For TRISO-coated small kernels (e.g., 350 μm diameter), an off-midplane correction based on shadow thickness resulted in an undesirably large error in the off-midplane correction. More recently, an alternate mathematical expression for ε based on the polish-down distance (p) was developed which can apply a small correction to mounts polished as near to average midplane as possible. Substituting in the mathematical expression for ε based on p, Eq. (1) was obtained for off-midplane correction of layer thickness [4]. Near midplane polishing minimizes the error in the as-measured radial positions of the layer boundaries; this minimized error is further reduced by the off-midplane correction based on p in order to provide highest accuracy for the calculated layer thickness. Note that particles with severe aspherical defects can violate the near-spherical assumption of Eq. (1) ($R \approx \varepsilon + p$), if the particle happens to be oriented with the defect on the polish surface of the mount. Fortunately, severe aspherical defects (diameter aspect ratio $>\sim 1.2$) are rare in conventional TRISO fuels.

Kernel radius measurement of cross-sectioned TRISO particles has additional technical difficulties which would require further refinements to procedures in order to provide high accuracy data. The radial position of the kernel/buffer boundary is the most affected by off-midplane polishing. Layer thicknesses are calculated by subtracting the corrected radial positions of two boundaries so any remaining bias in the radial boundary positions is largely cancelled out (because both boundary biases are in the same direction); kernel radius measurements only involve one layer boundary so any remaining bias in the kernel/buffer boundary fully affects the kernel radius measurements. Also, additional uncertainty in the off-midplane distance for the kernel can be caused by polishing behavior of the hard kernel compared to the surrounding TRISO composite structure. Certain kernels can react with the surrounding buffer during the coating process; this outer kernel surface can significantly fragment during polishing (even with backpotting) which causes uncertainty in the true boundary location. Shadow imaging kernels before coating can provide accurate radius results, so any effort to refine cross-sectional analysis for measuring kernel radius was deemed unnecessary.

Table 1 demonstrates the benefits of this off-midplane correction on the analysis of the buffer thickness of four particle batches and their associated composite material. The corrected average buffer thicknesses of these five materials varied from 108.9 μm to 114.1 μm (some variability likely due to coating process variability), while the as-measured (uncorrected) average buffer thicknesses varied from 109.7 μm to 115.7 μm. It was not uncommon for the buffer thickness correction for individual mounts to vary particle-to-particle from near zero to over −4 μm on the same mount.

The off-midplane corrections to IPyC, SiC, and OPyC thicknesses are smaller than the off-midplane corrections to the buffer thicknesses because of the greater radius at these layer boundaries. The average off-midplane corrections applied to the buffer, IPyC, SiC, and OPyC layer thicknesses of the mounts of these five materials were (respectively): −1.57 μm, −0.29 μm, −0.19 μm, and −0.19 μm.

5. Summary

Automated optical microscopy techniques developed at Oak Ridge National Laboratory provide dramatic improvements over conventional manual methods. In the shadow imaging of particles, hundreds of diameter measurements were made on each particle, and typical sample sizes were 1600–1800 for TRISO particles and 4000–5000 for kernels. In layer thickness measurements on cross-sectioned TRISO particles, hundreds of radial thickness measurements were made on each layer of each particle; sample size was typically 180–240 particles. In addition to the improvement in the determination of the mean and standard deviation of the distribution, the statistical analysis of optical microscopy data required for the qualification of TRISO fuel benefited from the large sample sizes made practical by automated methods. A mathematical correction was applied to layer thickness measurements on TRISO particle cross-sections in order to correct for off-midplane polishing, which was unavoidable by even meticulous conventional polishing methods.

Acknowledgements

Research was sponsored by the US-DOE Office of Nuclear Energy, Science, and Technology's Advanced Gas Reactor Fuel Development and Qualification program and by the Oak Ridge National Laboratory, managed by UT-Battelle, LLC for the US Department of Energy under Contract No. DE-AC05-00OR22725. All TRISO-coated particles discussed in this work were produced by Richard A. Lowden. Laboratory work by Ivan Dunbar, Deniz B. Aykac, and Andy Nelson contributed to the data collection and mount preparation included in this manuscript. All NUCO and LEUCO kernels used in this research were produced by Babcock and Wilcox Company in Lynchburg, Va.

References

[1] K. Verfondern (Ed.), 1997. Fuel Performance and Fission Product Behavior in Gas Cooled Reactors. IAEA Report IAEA-TECDOC-978.
[2] K. Sawa, S. Suzuki, S. Shiozawa, Nucl. Eng. Design 208 (2001) 305.
[3] C. Tang et al., J. Nucl. Sci. Technol. 37 (2000) 802.
[4] J.R. Price, D.B. Aykac, J.D. Hunn, A.K. Kercher, R.N. Morris, in: Proceedings of Machine Vision Applications in Industrial Inspection XIV, SPIE, vol. 6070, 2006, p. 60700H.
[5] J.R. Price, J.D. Hunn, in: Proceedings of Machine Vision Applications in Industrial Inspection XII, SPIE, vol. 5303, 2004, pp. 137–149.
[6] H. Nickel, H. Nabielek, G. Pott, A.W. Mehner, Nucl. Eng. Design 217 (2002) 141.
[7] D.A. Petti, J. Buongiorno, J.T. Maki, R.R. Hobbins, G.K. Miller, Nucl. Eng. Design 222 (2003) 281.
[8] P.J. Pappano, T.D. Burchell, J.D. Hunn, M.P. Trammel, in: Proceedings of the Seventh International Nuclear Graphite Specialist Meeting, J. Nucl. Mater., 2007.
[9] J.T. McClave, F.H. Dietrich, Statistics, fourth ed., Dellen, San Francisco, 1988. pp. 187, 363.
[10] R.H. McCuen, Statistical Methods for Engineers, Prentice-Hall, Englewood Cliffs NJ, 1985. pp. 22, 158, 403.